The Astrophysical Journal, 832:36 (9pp), 2016 November 20 doi:10.3847/0004-637X/832/1/36

RELATIVISTIC CYCLOTRON INSTABILITY IN ANISOTROPIC PLASMAS

Rodrigo A. López[1], Pablo S. Moya[1], Roberto E. Navarro[2], Jaime A. Araneda[2], Víctor Muñoz[1], Adolfo F. Viñas[3], and J. Alejandro Valdivia[1,4]
[1] Departamento de Física, Facultad de Ciencias, Universidad de Chile, Casilla 653, Santiago, Chile; rlopez186@gmail.com
[2] Departamento de Física, Facultad de Ciencias Físicas y Matemáticas, Universidad de Concepción, Casilla 160-C, Concepción, Chile
[3] NASA Goddard Space Flight Center, Heliophysics Science Division, Geospace Physics Laboratory, Mail Code 673, Greenbelt, MD 20771, USA
[4] Centro para el Desarrollo de la Nanociencia y Nanotecnología, CEDENNA, Chile
Received 2016 July 11; revised 2016 August 17; accepted 2016 August 22; published 2016 November 14

ABSTRACT

A sufficiently large temperature anisotropy can sometimes drive various types of electromagnetic plasma micro-instabilities, which can play an important role in the dynamics of relativistic pair plasmas in space, astrophysics, and laboratory environments. Here, we provide a detailed description of the cyclotron instability of parallel propagating electromagnetic waves in relativistic pair plasmas on the basis of a relativistic anisotropic distribution function. Using plasma kinetic theory and particle-in-cell simulations, we study the influence of the relativistic temperature and the temperature anisotropy on the collective and noncollective modes of these plasmas. Growth rates and dispersion curves from the linear theory show a good agreement with simulations results.

Key words: instabilities – methods: analytical – methods: numerical – plasmas – relativistic processes – waves

1. INTRODUCTION

A sufficiently large temperature anisotropy can sometimes drive various types of electromagnetic plasma micro-instabilities due to the available free energy (Gary 1993). Instabilities such as Weibel, whistler, mirror, firehose, or cyclotron are examples of anisotropy-driven instabilities and play an important role in the dynamics of the system in a wide range of environments that are related to space (Summers et al. 1998; Kasper et al. 2002; Bale et al. 2009), astrophysical (Schekochihin et al. 2005; Schlickeiser 2005; Riquelme et al. 2015), and laboratory (Lehnert 1967; Stenzel et al. 2007) plasmas. In a magnetized plasma, when the perpendicular temperature, $T_\perp$, (relative to the background magnetic field) exceeds the parallel temperature, $T_\parallel$, electromagnetic cyclotron waves propagating along the magnetic field can be excited, as long as the threshold condition for the cyclotron instability is fulfilled. This type of instability has been widely studied in space plasmas for ion (Otani 1988; Gary et al. 1996; Moya et al. 2011, 2012, 2014; Navarro et al. 2014b, 2015) and electron-driven waves (Gary & Wang 1996; Xiao et al. 1998; Viñas et al. 2015).

Relativistic analyses have been carried out to describe Weibel (Yoon 1989, 2007; Yang et al. 1993; Schaefer-Rolffs et al. 2006), firehose (Yoon 1990), and proton–cyclotron (Lazar & Schlickeiser 2006a) instabilities. The relativistic generalization becomes necessary in many laboratory and astrophysical situations, particularly situations in which electron–positron plasmas occur, such as ultra-intense lasers (Blaschke et al. 2006), active galactic nuclei (Reynolds et al. 1996; Hardy & Thoma 2000), bulk acceleration of relativistic jets (Iwamoto & Takahara 2002), quasar relativistic jets (Wardle et al. 1998), neutron star magnetospheres (Curtis 1991; Luo et al. 2002; Asseo 2003; Istomin & Sobyanin 2007), accretion disks (Bjöernsson et al. 1996), models of the early universe (Gibbons et al. 1990; Tajima & Taniuti 1990), among others. Recently, Sarri et al. (2015) report experimental evidence of the generation of high-density and neutral electron–positron plasma, opening the possibility of the study of pair plasmas in controlled laboratory experiments. Furthermore, a relativistic analysis is needed even in non-relativistic plasmas, such as in the case of collisionless damping for superluminal waves (Lazar & Schlickeiser 2003, 2004).

The aim of this work is to give a detailed description of the cyclotron instability in the relativistic regime, using both Vlasov linear theory and fully nonlinear particle simulations. We will solve the dispersion relation for parallel wave propagation in relativistic magnetized electron–positron plasmas, while also considering a relativistic anisotropic ($T_\perp \neq T_\parallel$) distribution function. Several alternatives including anisotropic effects in relativistic distributions have been proposed in the literature. For example, Yoon (1989) proposed an anisotropic distribution function that reduces to the Maxwell–Jüttner (Jüttner 1911) distribution in the isotropic limit and to the well-known Maxwell distribution in the non-relativistic limit. Another distribution was proposed by Schlickeiser (2004), which also satisfies the same limits. Other alternatives exist that include anisotropic effects in relativistic distributions (see for example Naito 2013; Stark et al. 2015; Treumann & Baumjohann 2015). However, the advantage of the one proposed by Schlickeiser (2004) is that the analytical continuation of the dispersion tensor can be calculated analytically (Lazar & Schlickeiser 2006a). Therefore, in this paper, we use the distribution function proposed by Schlickeiser (2004) to give an alternative derivation of the dispersion relation for anisotropic plasmas in the magnetized relativistic case, which is similar to the analysis provided by Lazar & Schlickeiser (2006a) and Schlickeiser et al. (2015), but we give numerical solutions of the completely relativistic dispersion relation in electron–positron plasmas with temperature anisotropy ($T_\perp > T_\parallel$). This paper presents an extension of the isotropic case studied in López et al. (2014a). Here, we study the growth rate of the cyclotron instability for different values of the plasma parameters. Particular relevance is given to the quasi-stable threshold conditions in the so-called relativistic temperature–anisotropy diagram. We also use a particle-in-cell (PIC) simulation to analyze the growth of this instability and its saturation, which are then compared to the results obtained from the linear theory.

This paper is organized as follows. In Section 2 we derive the linear dispersion relation for anisotropic plasmas. The dispersion relation is solved in Section 3 for a wide range of parameters, and in Section 4 we compare our results with PIC simulations. Finally, in Section 5, our results are summarized and conclusions are outlined.

2. LINEAR DISPERSION RELATION

Following López et al. (2014a), we start from the relativistic Vlasov equation to construct the linear dispersion relation for waves propagating parallel to the background magnetic field $\vec{B}_0 = B_0\hat{z}$ in an anisotropic plasma (Montgomery & Tidman 1964; Lerche 1967; Lazar & Schlickeiser 2003, 2006b). The transverse component of the dispersion tensor is given by

$$\Lambda^{+}_{R,L} = 1 - \frac{c^2k^2}{\omega^2} + \pi\sum_j \frac{\omega^2_{pj}}{\omega^2}\int_{-\infty}^{\infty} dp_z \int_0^{\infty} dp_\perp \times \frac{p_\perp^2}{\gamma\omega - kp_z/m_j \pm \Omega_j}\left[\left(\omega - \frac{kp_z}{m_j\gamma}\right)\frac{\partial f_j}{\partial p_\perp} + \frac{kp_\perp}{m_j\gamma}\frac{\partial f_j}{\partial p_z}\right], \quad (1)$$

where $\omega_{pj} = \sqrt{4\pi q_j^2 n_j/m_j}$ is the plasma frequency, q_j is the charge, n_j is the number density, m_j is the mass, $\Omega_j = q_jB_0/(m_jc)$ is the cyclotron frequency, and $f_j(p_z, p_\perp)$ is the one-particle distribution function for the species j, respectively. Also, c is the light speed, $p_\perp$ and p_z are the perpendicular and parallel components of the relativistic momentum, and $\gamma = \sqrt{1 + (p_\perp/m_jc)^2 + (p_z/m_jc)^2}$ is the relativistic Lorentz factor. Subscripts R and L in $\Lambda^{+}_{R,L}$ are the labels for right and left polarized waves, respectively. Notice that the right/left polarized waves correspond to the plus/minus sign in the resonant denominator, $\gamma\omega - kp_z/m \pm \Omega_j$, of Equation (1). Also, the wavefrequency is a complex number, $\omega = \omega_r + i\Gamma$, where ω_r is its real part and Γ is its imaginary part. The superindex $+$ in $\Lambda^{+}_{R,L}$ indicates that the dispersion relation Equation (1) is only valid for $\Gamma > 0$ (unstable waves).

We can rewrite Equation (1) using the transformation

$$s = p_z/(m_jc), \quad (2)$$

$$\gamma = \sqrt{1 + p_\perp^2/(m_jc)^2 + p_z^2/(m_jc)^2}, \quad (3)$$

where the determinant of the Jacobian matrix is

$$\det \mathrm{Jc} = \frac{\gamma(m_jc)^2}{\sqrt{\gamma^2 - 1 - s^2}}. \quad (4)$$

Then, Equation (1) becomes

$$\Lambda^{+}_{R,L} = 1 - \frac{c^2k^2}{\omega^2} - \pi\sum_j (m_jc)^3\frac{\omega^2_{pj}}{\omega^2}\int_1^{\infty} d\gamma \int_{-\sqrt{\gamma^2-1}}^{\sqrt{\gamma^2-1}} ds \times \left(\frac{\partial f_j}{\partial s} + \frac{\omega}{ck}\frac{\partial f_j}{\partial \gamma}\right)\frac{\gamma^2 - 1 - s^2}{s - \gamma\omega/(ck) \mp \Omega_j/(ck)}. \quad (5)$$

López et al. (2014a) gives a complete description of the dispersion relation for a plasma described by an isotropic Maxwell–Jüttner distribution function (Jüttner 1911). For the present work, we use the anisotropic relativistic velocity distribution function proposed by Schlickeiser (2004), namely

$$f_j(\gamma, s) = \frac{1}{4\pi(m_jc)^3 G(\mu_j, \alpha_j)}\, e^{-\mu_{\perp j}\gamma - \alpha_j s^2}. \quad (6)$$

Here $\mu_{\perp j}$ is a dimensionless parameter given by $\mu_{\perp j} = m_jc^2/(k_BT_{\perp j})$, where $T_{\perp j}$ is the temperature in the direction perpendicular to the background magnetic field and k_B is the Boltzmann constant. We also define $\mu_{\parallel j} = m_jc^2/(k_BT_{\parallel j})$, with $T_{\parallel j}$ as the parallel temperature. Thus, defining the temperature anisotropy as $A_j = T_{\perp j}/T_{\parallel j}$, we can write $\mu_{\parallel j} = A_j\mu_{\perp j}$.

To ensure the normalization of the distribution function (Equation (6)) we have defined the G function as

$$G(\mu_{\perp j}, \alpha_j) = \frac{1}{2}\sqrt{\frac{\pi}{\alpha_j}}\int_1^{\infty} \gamma\, \mathrm{Erf}(\sqrt{\alpha_j(\gamma^2 - 1)})e^{-\mu_{\perp j}\gamma}\, d\gamma, \quad (7)$$

where $\mathrm{Erf}(x)$ is the error function. In Equation (6), α_j is related to the temperature anisotropy of the distribution of species j. As mentioned by Schlickeiser (2004), the choice of this distribution is convenient because in the limit $\alpha_j \to 0$, we obtain

$$\lim_{\alpha_j\to 0}\frac{1}{\sqrt{\alpha_j}}\mathrm{Erf}(\sqrt{\alpha_j(\gamma^2 - 1)}) = \frac{2}{\sqrt{\pi}}\sqrt{\gamma^2 - 1}, \quad (8)$$

and we recover the well-known Maxwell–Jüttner distribution. Also, in the non-relativistic limit, the distribution defined by Equation (6) can be well approximated by a bi-Maxwellian distribution as long as the anisotropic parameter can be interpreted as (Schlickeiser 2004)

$$\alpha_j = \frac{\mu_{\perp j}}{2}(A_j - 1). \quad (9)$$

Now, by replacing the distribution function (Equation (6)), in the dispersion tensor (Equation (5)), we obtain

$$\Lambda^{+}_{R,L} = 1 - \frac{1}{z^2} + \sum_j \frac{1}{4G(\mu_{\perp j}, \alpha_j)}\frac{\omega^2_{pj}}{c^2k^2z^2}\int_1^{\infty} d\gamma\, e^{-\mu_{\perp j}\gamma} \times \{M^{+}_{R,L;j}(\gamma) + N^{+}_{R,L;j}(\gamma)\}, \quad (10)$$

where we have defined

$$M^{+}_{R,L;j}(\gamma) = 2\alpha_j\int_{-\sqrt{\gamma^2-1}}^{\sqrt{\gamma^2-1}} s\,\frac{\gamma^2 - 1 - s^2}{s - \gamma z \mp t_j}e^{-\alpha_j s^2}\, ds, \quad (11)$$

$$N^{+}_{R,L;j}(\gamma) = z\mu_{\perp j}\int_{-\sqrt{\gamma^2-1}}^{\sqrt{\gamma^2-1}} \frac{\gamma^2 - 1 - s^2}{s - \gamma z \mp t_j}e^{-\alpha_j s^2}\, ds, \quad (12)$$

with $z = \omega/(ck)$ and $t_j = \Omega_j/(ck)$.

Following the procedure described in the Appendix, we can reduce the integrals in Equations (11) and (12) to

$$\begin{aligned} M^{+}_{R,L;j}(\gamma) = 2\alpha_j[&(1-z^2)z\gamma^3 \mp (3z^2-1)t_j\gamma^2 \\ &- (1+3t^2)z\gamma \mp (1+t_j^2)t_j]J^{+}_{R,L;j}(\gamma) \\ &+ 2\alpha_j[(1-z^2)\gamma^2 \mp 2zt_j\gamma - (1+t_j^2)] \\ &\times \sqrt{\frac{\pi}{\alpha_j}}\,\mathrm{Erf}(\sqrt{\alpha_j(\gamma^2-1)}) \\ &- \sqrt{\frac{\pi}{\alpha_j}}\,\mathrm{Erf}(\sqrt{\alpha_j(\gamma^2-1)}) \\ &+ 2\sqrt{\gamma^2-1}\; e^{-\alpha_j(\gamma^2-1)}, \end{aligned} \tag{13}$$

$$\begin{aligned} N^{+}_{R,L;j}(\gamma) = z\mu_{\perp j}[&(1-z^2)\gamma^2 \mp 2\gamma t_j z - (1+t^2)]J^{+}_{R,L;j}(\gamma) \\ &- z\mu_{\perp j}(\gamma z \pm t_j)\sqrt{\frac{\pi}{\alpha_j}}\,\mathrm{Erf}(\sqrt{\alpha_j(\gamma^2-1)}), \end{aligned} \tag{14}$$

where

$$J^{+}_{R,L;j}(\gamma) = \int_{-\sqrt{1-\gamma^{-2}}\mp t_j/\gamma}^{\sqrt{1-\gamma^{-2}}\mp t_j/\gamma} \frac{e^{-\alpha_j(\gamma\eta\pm t_j)^2}}{\eta - z}\, d\eta. \tag{15}$$

In the isotropic limit, $\alpha_j = 0$, we recover the results obtained by López et al. (2014a). Indeed, in this limit and because of Equation (8), we obtain $M^{+}_{R,L;j}(\gamma) = 0$, whereas $N^{+}_{R,L;j}(\gamma)$ and $J^{+}_{j}(\gamma)$ reduce to Equations (11) and (12) defined in López et al. (2014a), respectively.

In the anisotropic case, the integral given by Equation (15) can be rewritten as

$$\begin{aligned} J^{+}_{R,L;j}(\gamma) = &\ln\left(\frac{z - \sqrt{1-\gamma^{-2}} \pm t_j/\gamma}{z + \sqrt{1-\gamma^{-2}} \pm t_j/\gamma}\right) e^{-\alpha_j(\gamma^2-1)} \\ &+ 2\alpha_j\gamma \int_{-\sqrt{1-\gamma^{-2}}\mp t_j/\gamma}^{\sqrt{1-\gamma^{-2}}\mp t_j/\gamma} (\gamma\eta \pm t_j) \\ &\times \ln(\eta - z) e^{-\alpha_j(\gamma\eta\pm t_j)^2}\, d\eta. \end{aligned} \tag{16}$$

Thus, the dispersion tensor in Equation (10) can be computed as a single integral in γ (see López et al. 2014a), plus a new term that vanishes when the distribution is isotropic ($\alpha_j = 0$).

The dispersion tensor (Equation (10)) is valid for the upper complex frequency plane only ($\mathrm{Im}(\omega) = \Gamma > 0$). The proper analytical continuation to $\Lambda^{-}_{R,L}$ for $\Gamma < 0$ defines a dispersion tensor in the whole complex frequency plane. In this case, we require that

$$\lim_{\Gamma\to 0^+} \Lambda^{+}_{R,L} = \lim_{\Gamma\to 0^-} \Lambda^{-}_{R,L}, \tag{17}$$

which is equivalent to finding the analytical continuation $J^{-}_{R,L;j}$ of the integral $J^{+}_{R,L;j}$, i.e.,

$$\lim_{\Gamma\to 0^+} J^{+}_{R,L;j} = \lim_{\Gamma\to 0^-} J^{-}_{R,L;j}. \tag{18}$$

Equation (16) depends on the complex logarithmic function. For the principal branch of the logarithm, this equation will be valid for the entire complex frequency plain, but excludes the negative values of the real part of the frequency, $\omega_r < 0$. To evaluate the logarithm function in these cases, we can use the analytic continuation given by López et al. (2014a; also see Schlickeiser et al. 2015), so that Equation (10) becomes valid in the entire complex frequency plane. Therefore, we can remove the $+$ superscript in $\Lambda^{+}_{R,L}$ and obtain the dispersion tensor $\Lambda_{R,L}$:

$$\begin{aligned} \Lambda_{R,L} = 1 - \frac{c^2k^2}{\omega^2} + \sum_j \frac{1}{4G(\mu_{\perp j}, \alpha_j)}\frac{\omega_{pj}^2}{\omega^2}\int_1^\infty d\gamma\; e^{-\mu_{\perp j}\gamma} \\ \times \{M_{R,L;j}(\gamma) + N_{R,L;j}(\gamma)\}, \end{aligned} \tag{19}$$

which is well defined for any complex frequency.

3. NUMERICAL ANALYSIS

A closed form for Equation (19) in terms of known functions has not yet been found. Instead, we obtained solutions of the dispersion relation by solving numerically in Equations (16) and (19) using adaptive integration methods. We focus our attention on the left polarized component of the dispersion tensor, Λ_L, to study the propagation of Alfvén waves through a relativistic pair plasma composed of electrons and positrons, $m = m_e = m_p$ (Equation (19) is general and valid for a plasma composed of any kind of particles). In Figure 1 we plotted the solutions of the dispersion relation, $\Lambda_L = 0$, for $\omega_{pe}/\Omega_c = 1$, and for several temperatures and temperature anisotropies. Figure 1(a) shows the real part of the dispersion relation (ω_r/Ω_c versus ck/Ω_c) for $\mu_{\perp p} = \mu_{\perp e} = 50$, $A_e = 1.0$, and several positron anisotropies ($A_p = 1.0, 2.0, 5.0, 7.0, 10.0$). We have chosen isotropic electrons and anisotropic positrons. In this case, the free energy is stored in the positrons' distribution, therefore an Alfvén positron–cyclotron instability is expected to occur. We focus our attention in the first quadrant of the dispersion diagram (ω_r, $k > 0$) for the left dispersion relation because that quadrant shows the waves resonating with the positrons. As the electrons are isotropic, electron-driven instability is not expected to occur, and we will only see the normal modes in the third and fourth quadrants ($\omega_r < 0$). The right component (whistler waves) can also be obtained by changing $\omega_r \to -\omega_r$ (López et al. 2014a; Schlickeiser et al. 2015), and in that case, the waves resonating with the electrons will be in the first and second quadrants. Furthermore, to study the whistler–cyclotron instability, we would have to introduce a temperature anisotropy in the electron distribution. Given the symmetry of the dispersion tensor, the results would be equivalent. Figure 1(b) displays the corresponding imaginary part Γ/Ω_c versus ck/Ω_c. For $A_p = 1.0$ (black line), we recover the isotropic case shown in López et al. (2014a), in which the Alfvén branch is stable until $ck/\Omega_c \sim 1$ and becomes damped with increasing damping for increasing values of the wavenumber. The figure also shows that for the same temperature and a positron anisotropy of $A_p = 2.0$, the waves become damped for larger values of the wavenumbers (blue curve). In addition, from the figure we can also see that an instability $\Gamma(k) > 0$ occurs for values of the positron anisotropy $A_p > 2$, so that the unstable range of wavenumbers, as well as the maximum growth rate, become wider for larger positron anisotropies. Figures 1(c) and (d) are equivalent to Figures 1(a) and (b), but for $\mu_{\perp e} = \mu_{\perp p} = 10$. Similarly, Figures 1(e) and (f) are equivalent to Figures 1(a) and (b), but for $\mu_{\perp e} = \mu_{\perp p} = 2$. From these figures, we can appreciate that as the perpendicular temperature increases, the instability occurs for smaller wavenumbers, while the growth rates and associated range of unstable wavenumbers become larger.

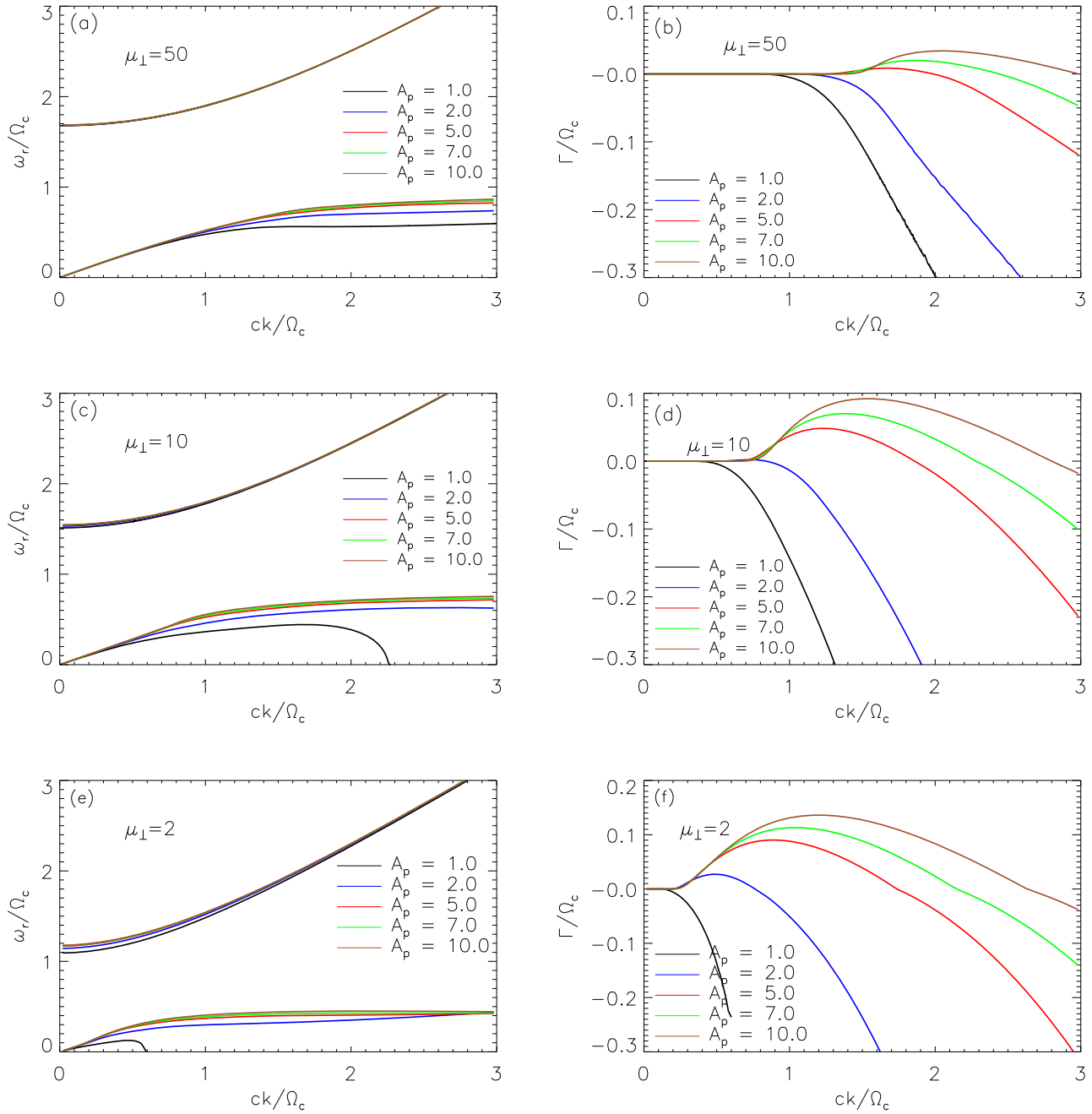

Figure 1. Dispersion relation $\Lambda_L = 0$ for $\omega_{pe}/\Omega_c = 1$ and $A_e = 1$. (a) Normalized real part of the frequency ω_r/Ω_c vs. normalized wavenumber ck/Ω_c, for $\mu_{\perp e} = \mu_{\perp p} = 50$, and several anisotropies for the positrons A_p. (b) Normalized imaginary part of the frequency Γ/Ω_c vs. normalized wavenumber ck/Ω_c, for $\mu_{\perp e} = \mu_{\perp p} = 50$, and several values of A_p. (c) Same as (a) but for $\mu_{\perp e} = \mu_{\perp p} = 10$. (d) Same as (b) but for $\mu_{\perp e} = \mu_{\perp p} = 10$. (e) Same as (a) but for $\mu_{\perp e} = \mu_{\perp p} = 2$. (f) Same as (b) but for $\mu_{\perp e} = \mu_{\perp p} = 2$.

To study the relation between growth rate, temperature, and anisotropy, we find the maximum growth rate of the Alfvén mode for several combinations of $\mu_{\perp p}$ and A_p. Figure 2(a) clearly shows the dependence of the maximum growth rate, $\Gamma_{\max}/\Omega_c$, on the perpendicular thermal factor, $\mu_{\perp p} = mc^2/(k_B T_{\perp p})$. The maximum growth rate is larger for larger anisotropies, and grows rapidly with the positron perpendicular temperature for large temperatures (small $\mu_{\perp p}$). The same dependence is found for the parallel thermal factor $\mu_{\|p}$, as it is shown in Figure 2(b). In both panels, we have drawn up to a threshold limit for the Alfvén cyclotron instability given by $\Gamma_{\max}/\Omega_c = 10^{-3}$. This limit is equivalent to the commonly used threshold for ion–cyclotron waves in non-relativistic plasmas (Bale et al. 2009; Navarro et al. 2014b, 2015), showing that the free energy necessary to excite cyclotron waves is inversely proportional to the plasma temperature. Thus, the process involved in this micro-instability for the non-relativistic case remains in the relativistic regime. In Figure 2(b), we have cut from the zone above the dashed line because that zone corresponds to ultra-relativistic temperatures, $\mu_{\perp p} < 1$. In that limit, there are several other effects that could become important for the dynamics of the plasmas, such as pair creation or annihilation, photon–particle (anti-particle) collisions, and

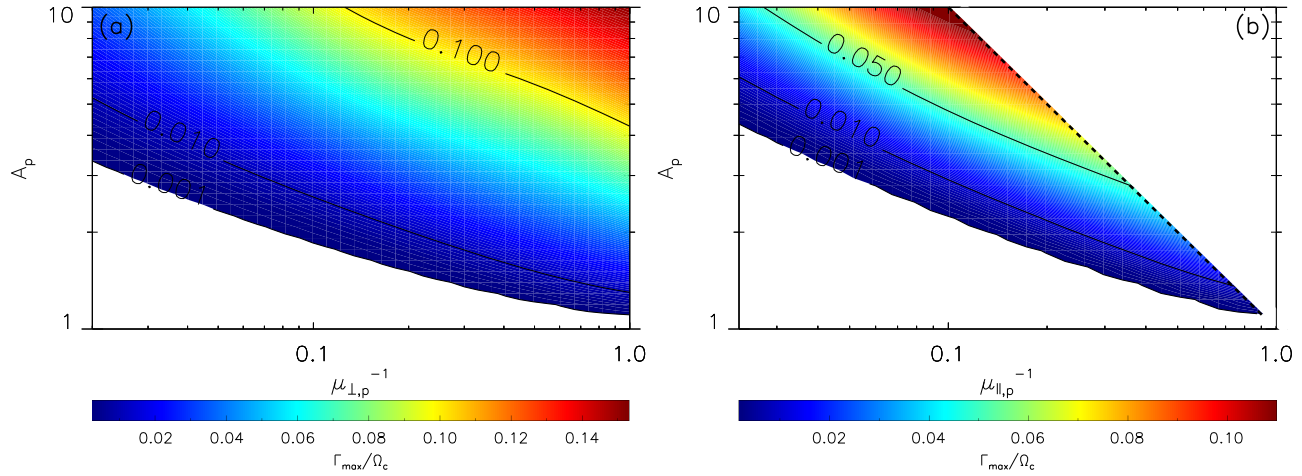

Figure 2. Maximum growth rate, $\Gamma_{\max}/\Omega_c$, as a function of: (a) normalized perpendicular temperature $\mu_{\perp p}^{-1}$ and the positron anisotropy A_p, (b) normalized parallel temperature $\mu_{\|p}^{-1}$ and the positron anisotropy. Both figures were computed for $\omega_{pe}/\Omega_c = 1$, $A_e = 1$ and $\mu_{\perp e} = \mu_{\perp p}$. The dashed line defines the limit $\mu_{\perp p} = 1$.

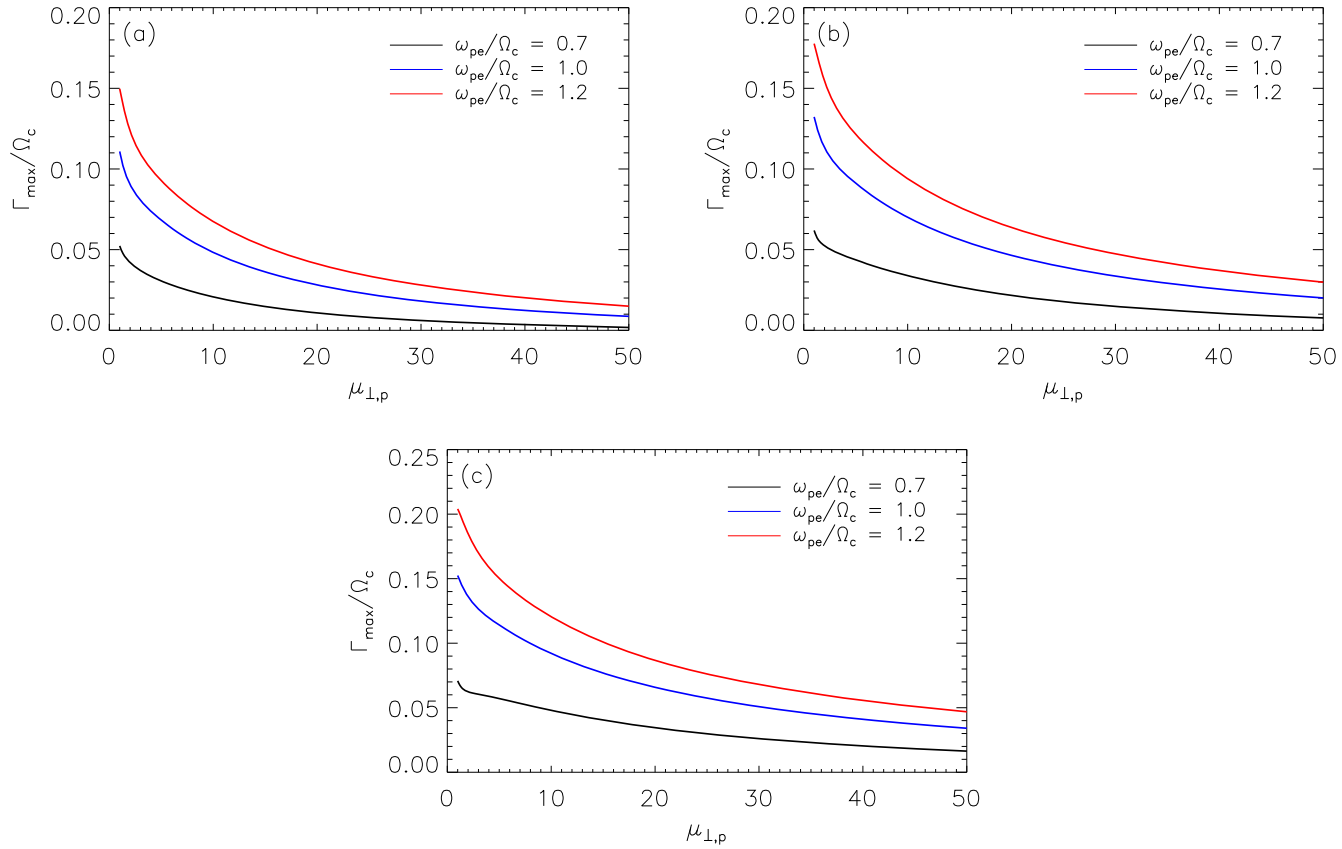

Figure 3. Maximum growth rate $\Gamma_{\max}/\Omega_c$ as a function of normalized perpendicular parameter $\mu_{\perp p}$, for several values of ω_{pe}/Ω_c and $A_e = 1$. (a) $A_p = 5$. (b) $A_p = 7$. (c) $A_p = 10$.

photon related effects, which are beyond the scope of this paper.

Finally, the growth rate dependence on the parameter ω_{pe}/Ω_c is shown in Figure 3. Here we present three cuts of Figure 2(a) at anisotropies $A_p = 5$ in Figure 3(a), $A_p = 7$ in Figure 3(b), and $A_p = 10$ in Figure 3(c); all figures for three different values of ω_{pe}/Ω_c. It is clear that for a given positron anisotropy, the growth rate increases as the parameter ω_{pe}/Ω_c increases, for the whole range of $\mu_{\perp p}$ shown. Namely, as the positron beta β_p can be written as $\beta_p = (2/\mu_p)(\omega_{pe}/\Omega_c)^2$, plasmas with a larger ω_{pe}/Ω_c ratio correspond to denser plasmas with larger β_p, and the plasma is more unstable for the same anisotropy value.

4. PARTICLE IN CELL SIMULATIONS

We now study the evolution of the cyclotron instability using electron–positron one-dimensional relativistic PIC simulations. The detailed description of the simulation scheme is given in López et al. (2014b, 2015a), so here we only present the simulation parameters. In this case, the system size is $L = 512$ (in units of the electron inertial length ω_{pe}/c), the number of

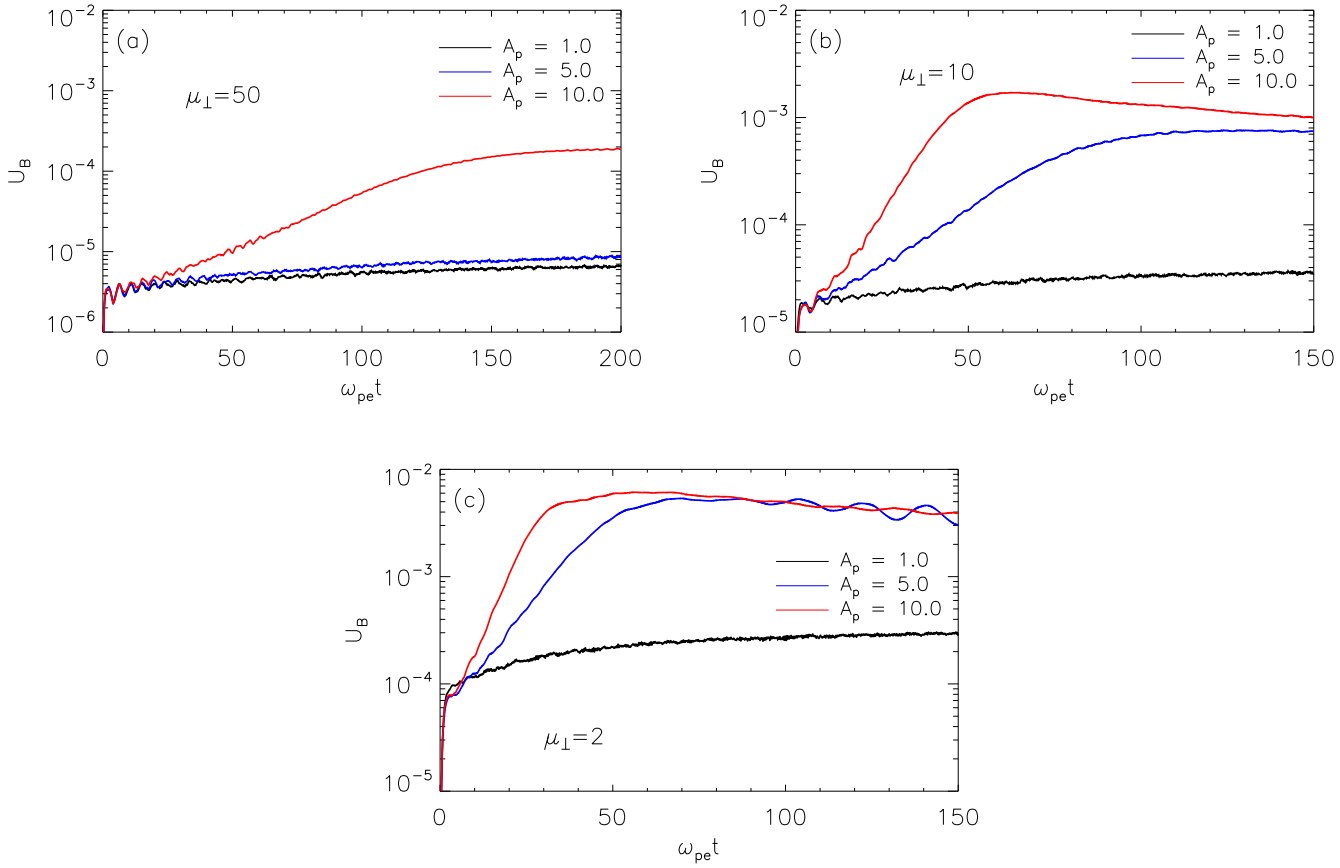

Figure 4. Temporal evolution of the normalized transverse magnetic energy, U_B, for $\omega_{pe}/\Omega_c = 1$, $A_e = 1$, and $\mu_{\perp e} = \mu_{\perp p}$, (a) $\mu_{\perp p} = 50$, (b) $\mu_{\perp p} = 10$, and (c) $\mu_{\perp p} = 2$.

spatial grid points is $n_g = 2048$, the number of particles per grid is $n_p = 1000$, the time step is $\omega_{pe}\Delta t = 0.01$, and the simulation runs until $\omega_{pe}t_{\max} = 655.36$. We start our simulations from a quiet state, in which the particle velocities are only given by their thermal motion obtained from the anisotropic version of the Maxwell–Jüttner distribution function, which is discussed in Section 3.

Figure 4 shows the temporal evolution of the transverse magnetic field energy, U_B, using $A_e = 1$ and $\omega_{pe}/\Omega_c = 1$ for three different initial positron temperatures and three values of the anisotropy. For all temperatures, the isotropic case $A_p = 1$ is represented by black lines in the figure. Even in the absence of free energy in the form of temperature anisotropy, we observe that the field energy has a slow temporal growth due to the self-generation of spontaneous thermally induced fluctuations. The level of these fluctuations increases with the temperature as predicted by Navarro et al. (2014a) and López et al. (2015b). In Figure 4 we also show anisotropic cases with available free energy at the beginning of the simulation. For $A_p \neq 1$, we observe an instability growth that depends on the temperature of the plasma. Figure 4(a) shows the case for low temperature, $\mu_{\perp p} = 50$, in which the initial anisotropy $A_p = 5$ is not large enough to excite the instability during the interval covered by the simulation; i.e., the system is in a quasi-stable state with a very small growth rate, which is consistent with Figure 2. Indeed, according to Figure 2(a), the normalized maximum growth rate is below 10^{-2}, and then the system approaches a state in which there is a balance between thermally induced electromagnetic fluctuations and dissipation. However, for the same temperature but for $A_p = 10$, we can observe the triggering of the linear cyclotron instability. In the initial stage of the simulation, we observe an exponential growth, giving rise to a saturation of the magnetic energy for larger times. Figures 4(b) and (c) show cases with $\mu_{\perp p} = 10$ and $\mu_{\perp p} = 2$, respectively. As the temperature and anisotropy increase, the plasma is more unstable and the system reaches the saturation level more quickly.

Finally, in Figure 5, we show the power spectrum of the transverse magnetic fluctuations. For a better comparison, we have superimposed the numerical dispersion relation $|\Lambda_L| = 0$ (Equation (19)) as a solid black line. Dashed and dotted black lines represent the numerical solution with $\Gamma/\Omega_c > 10^{-4}$ (unstable range) and $\Gamma/\Omega_c < -10^{-4}$ (damped range), respectively. Figure 5(a) shows the case for $\mu_{\perp p} = 50$ and $A_p = 5$. We observe a good agreement between the normal modes obtained from a direct solution of the dispersion relation and modes that appear in the fully nonlinear simulations. For this temperature and anisotropy, the instability range is narrow ($1.2 < ck/\Omega_p < 2.0$) and the maximum growth rate is very small, so that the thermally induced electromagnetic fluctuations can be observed in the spectrum. This spectrum is similar to the ones obtained in the isotropic case (López et al. 2014a, 2015b). In Figure 5(b), we show the case with $A_p = 10$. Now the power in the spectrum is concentrated in the unstable branch with a level that is much larger than that of the fluctuations, which is also in good agreement with the theory. For larger temperatures (Figures 5(c) and (d)), the power in the

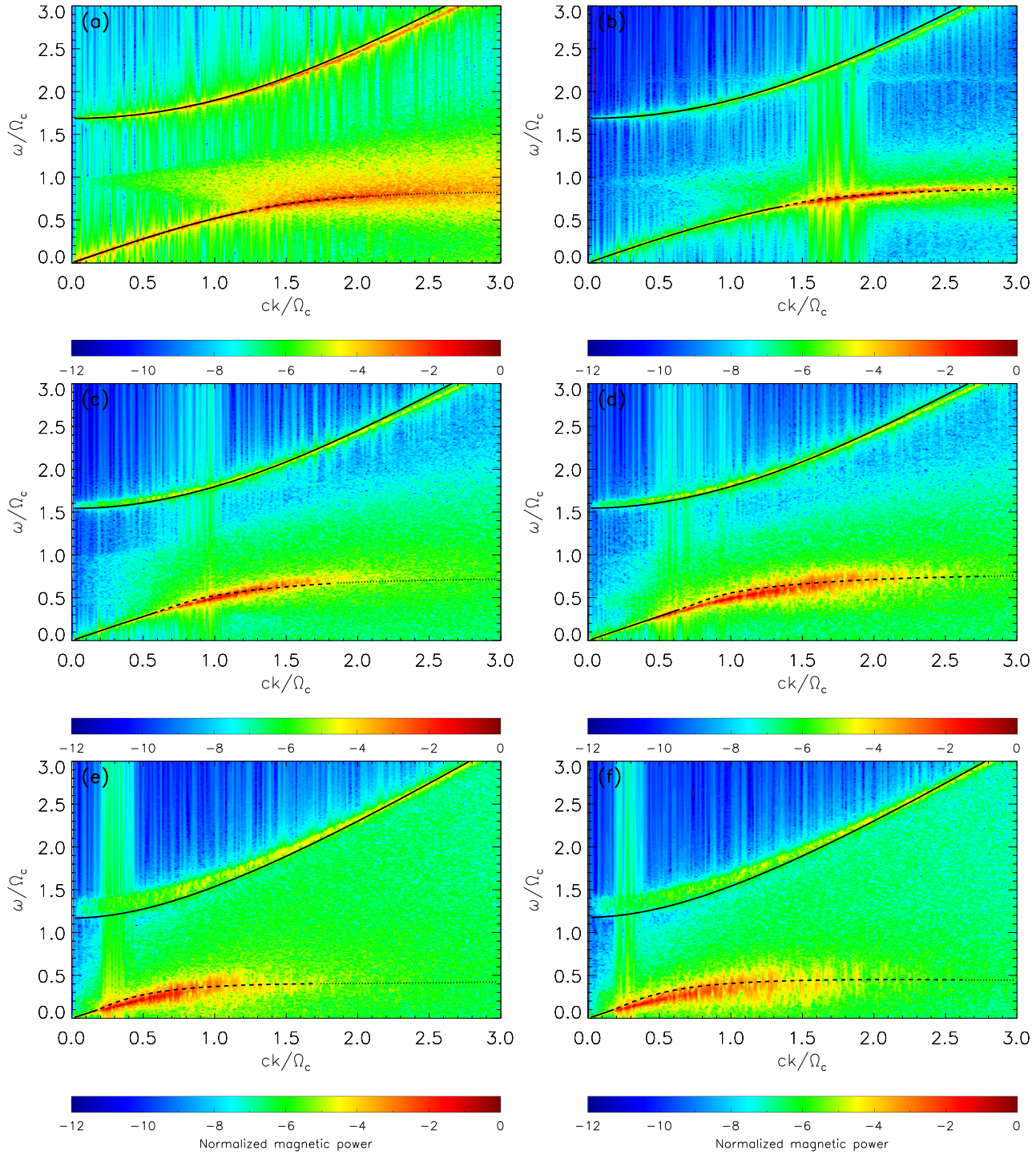

Figure 5. Power spectrum of the normalized magnetic field fluctuations obtained from the PIC simulations, for $\omega_{pe}/\Omega_c = 1$, $A_e = 1$. $\mu_{\perp e} = \mu_{\perp p}$. (a) $\mu_{\perp p} = 50$ and $A_p = 5$. (b) $\mu_{\perp p} = 50$ and $A_p = 10$. (c) $\mu_{\perp p} = 10$ and $A_p = 5$. (d) $\mu_{\perp p} = 10$ and $A_p = 10$. (e) $\mu_{\perp p} = 2$ and $A_p = 5$. (f) $\mu_{\perp p} = 2$ and $A_p = 10$. The real part of the numerical dispersion relation $\Lambda_L = 0$ has been superimposed as a black line in all figures. The solid line represents the numerical solution with $|\Gamma|/\Omega_c < 10^{-4}$; the dashed line is the numerical solution with $\Gamma/\Omega_c > 10^{-4}$; the dotted line is the numerical solution with $\Gamma/\Omega_c < -10^{-4}$.

instability branch becomes greater and the instability range becomes larger.

5. CONCLUSIONS

We have studied the relativistic electron–positron–cyclotron instability by means of a covariant kinetic linear theory and PIC simulations using a relativistic anisotropic distribution function first proposed by Schlickeiser (2004), which reduces to the Maxwell–Jüttner distribution in the isotropic limit and to the bi-Maxwellian distribution in the non-relativistic limit. For this distribution function, we found analytic expressions for the complex dispersion tensor using an analytic continuation technique, and we were able to study unstable and damped

solutions of the dispersion relation. We studied numerically the relativistic dispersion relation and the growth rate of the cyclotron instability for a wide range of temperatures and anisotropies of the plasma. In the absence of temperature anisotropy, all our expressions reduce to the isotropic case studied in López et al. (2014a).

Using linear theory, we estimated the instability threshold for the maximum growth rate of the positron–cyclotron mode as a function of the parallel and perpendicular temperatures, and found that the behavior of the instability as a function of temperature anisotropy and the μ parameter is similar to the well-known anisotropy-beta diagram for cyclotron waves in non-relativistic plasmas (Bale et al. 2009; Navarro et al. 2014b). Finally, using PIC simulations, we analyze the evolution of this instability and its imprint on the spectrum of the magnetic field, and obtain good agreement between linear theory and nonlinear simulations. Furthermore, our simulations show the possibility of coexistence of normal modes and spontaneous thermally induced electromagnetic fluctuations for several ranges of the plasma parameters.

Both the existence of a quasi-stable state with a finite level of thermally induced electromagnetic fluctuations and the analysis of the nonlinear saturation of the instability will be analyzed in detail in future manuscripts.

Our results may be relevant for the understanding of astrophysical relativistic magnetized plasma environments, in which some degree of temperature anisotropy is expected, and therefore wave–particle interactions and kinetic instability thresholds may be relevant for the dynamics of the system.

We thank CONICyT through FONDECyT Grants No. 1150718 and No. 1130273 (J.A.V.); No. 1161711 (V.M.); No. 1161700 (J.A.A.); No. 11150055 (P.S.M.); and FONDECyT Postdoctoral Grant No. 3150262 (R.E.N.). We also thank CEDENNA and CONICyT PIA project ACT1405 for their financial support. A.F.V. would like to thank the NASA-Wind/SWE project for their support. J.A.A. also thanks the Universidad de Concepción for support through VRID-Enlace grant No. 215.011.059-1.0.

APPENDIX
CALCULATION OF $M^{+}_{R,L;j}$ AND $N^{+}_{R,L;j}$

Using the substitution $\eta = (s \mp t_j)/\gamma$ in Equations (11) and (12), we obtain

$$M^{+}_{R,L;j}(\gamma) = 2\alpha_j \int_{-\sqrt{1-\gamma^{-2}}\mp t_j/\gamma}^{\sqrt{1-\gamma^{-2}}\mp t_j/\gamma} \times \frac{\pm(\gamma^2 - 1 - t_j^2)t_j + \gamma(\gamma^2 - 1 - 3t_j^2)\eta \mp 3\gamma^2 t_j\eta^2 - \gamma^3\eta^3}{\eta - z} \times e^{-\alpha_j(\gamma\eta\pm t_j)^2} d\eta, \tag{20}$$

$$N^{+}_{R,L;j}(\gamma) = z\mu_{\perp j} \int_{-\sqrt{1-\gamma^{-2}}\mp t_j/\gamma}^{\sqrt{1-\gamma^{-2}}\mp t_j/\gamma} \times \frac{(\gamma^2 - 1 - t_j^2) \mp 2\gamma t_j\eta - \gamma^2\eta^2}{\eta - z} e^{-\alpha_j(\gamma\eta\pm t_j)^2} d\eta. \tag{21}$$

Then, in order to reduce these expressions, we use the following integral relations:

$$\int_{-\sqrt{1-\gamma^{-2}}\mp t_j/\gamma}^{\sqrt{1-\gamma^{-2}}\mp t_j/\gamma} e^{-\alpha_j(\gamma\eta\pm t_j)^2} d\eta = \frac{1}{\gamma}\sqrt{\frac{\pi}{\alpha_j}}\,\mathrm{Erf}(\sqrt{\alpha_j(\gamma^2-1)}), \tag{22}$$

$$\int_{-\sqrt{1-\gamma^{-2}}\mp t_j/\gamma}^{\sqrt{1-\gamma^{-2}}\mp t_j/\gamma} \eta e^{-\alpha_j(\gamma\eta\pm t_j)^2} d\eta = \mp\frac{t_j}{\gamma^2}\sqrt{\frac{\pi}{\alpha_j}}\,\mathrm{Erf}(\sqrt{\alpha_j(\gamma^2-1)}), \tag{23}$$

$$\int_{-\sqrt{1-\gamma^{-2}}\mp t_j/\gamma}^{\sqrt{1-\gamma^{-2}}\mp t_j/\gamma} \eta^2 e^{-\alpha_j(\gamma\eta\pm t_j)^2} d\eta = -\frac{\sqrt{\gamma^2-1}}{\alpha_j\gamma^3} e^{-\alpha_j(\gamma^2-1)} + \frac{1}{\gamma^3}\sqrt{\frac{\pi}{\alpha_j}}\left(\frac{1}{2\alpha_j} + t_j^2\right)\mathrm{Erf}(\sqrt{\alpha_j(\gamma^2-1)}). \tag{24}$$

$$\int_{-\sqrt{1-\gamma^{-2}}\mp t_j/\gamma}^{\sqrt{1-\gamma^{-2}}\mp t_j/\gamma} \eta\,\frac{e^{-\alpha_j(\gamma\eta\pm t_j)^2}}{\eta - z} d\eta = zJ^{+}_{R,L;j}(\gamma) + \frac{1}{\gamma}\sqrt{\frac{\pi}{\alpha_j}}\,\mathrm{Erf}(\sqrt{\alpha_j(\gamma^2-1)}), \tag{25}$$

$$\int_{-\sqrt{1-\gamma^{-2}}\mp t_j/\gamma}^{\sqrt{1-\gamma^{-2}}\mp t_j/\gamma} \eta^2\,\frac{e^{-\alpha_j(\gamma\eta\pm t_j)^2}}{\eta - z} d\eta = z^2J^{+}_{R,L;j}(\gamma) + \frac{1}{\gamma^2}\sqrt{\frac{\pi}{\alpha_j}}\,(\gamma z \mp t_j)\mathrm{Erf}(\sqrt{\alpha_j(\gamma^2-1)}), \tag{26}$$

$$\int_{-\sqrt{1-\gamma^{-2}}\mp t_j/\gamma}^{\sqrt{1-\gamma^{-2}}\mp t_j/\gamma} \eta^3\,\frac{e^{-\alpha_j(\gamma\eta\pm t_j)^2}}{\eta - z} d\eta = \frac{1}{\gamma}\sqrt{\frac{\pi}{\alpha_j}}\left(z^2 \mp \frac{zt_j}{\gamma} + \frac{1}{2\alpha_j\gamma^2} + \frac{t^2}{\gamma^2}\right) \times \mathrm{Erf}(\sqrt{\alpha_j(\gamma^2-1)}) - \frac{\sqrt{\gamma^2-1}}{\alpha_j\gamma^3} e^{-\alpha_j(\gamma^2-1)} + z^3J^{+}_{R,L;j}(\gamma). \tag{27}$$

Thus, by replacing Equations (22)–(27) in Equations (20) and (21), we obtain the expressions in Equations (13) and (14).

REFERENCES

Asseo, E. 2003, PPCF, 45, 853
Bale, S. D., Kasper, J. C., Howes, G. G., et al. 2009, PhRvL, 103, 211101
Björnsson, G., Abramowicz, M. A., Chen, X., & Lasota, J.-P. 1996, ApJ, 467, 99
Blaschke, D. B., Prozorkevich, A. V., Roberts, C. D., Schmidt, S. M., & Smolyansky, S. A. 2006, PhRvL, 96, 140402
Curtis, M. F. 1991, The Theory of Neutron Stars Magnetospheres (Chicago: Univ. Chicago Press)
Gary, S. P. 1993, Theory of Space Plasma Microinstabilities (Cambridge: Cambridge Univ. Press)
Gary, S. P., Vazquez, V. M., & Winske, D. 1996, JGR, 101, 13327
Gary, S. P., & Wang, J. 1996, JGR, 101, 10749
Gibbons, G. W., Hawking, S., & Siklos, S. T. C. 1990, The Very Early Universe (Cambridge: Cambridge Univ. Press)
Hardy, S. J., & Thoma, M. H. 2000, PhRvD, 63, 025014

Istomin, Y. N., & Sobyanin, D. N. 2007, AstL, 33, 660
Iwamoto, S., & Takahara, F. 2002, ApJ, 565, 163
Jüttner, F. 1911, AnPhy, 339, 856
Kasper, J. C., Lazarus, A. J., & Gary, S. P. 2002, GeoRL, 29, 1839
Lazar, M., & Schlickeiser, R. 2003, CaJPh, 81, 1377
Lazar, M., & Schlickeiser, R. 2004, PhyS, 2004, 130
Lazar, M., & Schlickeiser, R. 2006a, PhPl, 13, 012110
Lazar, M., & Schlickeiser, R. 2006b, NJPh, 8, 66
Lehnert, B. 1967, PlPh, 9, 301
Lerche, I. 1967, ApJ, 147, 689
López, R. A., Moya, P. S., Muñoz, V., Viñas, A. F., & Valdivia, J. A. 2014a, PhPl, 21, 092107
López, R. A., Muñoz, V., Viñas, A. F., & Valdivia, J. A. 2014b, PhPl, 21, 032102
López, R. A., Muñoz, V., Viñas, A. F., & Valdivia, J. A. 2015a, PhPl, 22, 092115
López, R. A., Navarro, R. E., Moya, P. S., et al. 2015b, ApJ, 810, 103
Luo, Q., Melrose, D., & Fussell, D. 2002, PhRvE, 66, 026405
Montgomery, D., & Tidman, D. 1964, Plasma Kinetic Theory (New York: McGraw-Hill)
Moya, P. S., Muñoz, V., Rogan, J., & Valdivia, J. A. 2011, JASTP, 73, 1390
Moya, P. S., Navarro, R., Viñas, A. F., Muñoz, V., & Valdivia, J. A. 2014, ApJ, 781, 76
Moya, P. S., Viñas, A. F., Muñoz, V., & Valdivia, J. A. 2012, AnGeo, 30, 1361
Naito, O. 2013, PhPl, 20, 044501
Navarro, R. E., Araneda, J. A., Muñoz, V., et al. 2014a, PhPl, 21, 092902
Navarro, R. E., Moya, P. S., Muñoz, V., et al. 2014b, PhRvL, 112, 245001
Navarro, R. E., Muñoz, V., Araneda, J. A., et al. 2015, JGR, 120, 2382
Otani, N. F. 1988, JCoPh, 78, 251
Reynolds, C. S., Fabian, A. C., Celotti, A., & Rees, M. J. 1996, MNRAS, 283, 873
Riquelme, M. A., Quataert, E., & Verscharen, D. 2015, ApJ, 800, 27
Sarri, G., Poder, K., Cole, J. M., et al. 2015, NatCo, 6, 6747
Schaefer-Rolffs, U., Lerche, I., & Schlickeiser, R. 2006, PhPl, 13, 012107
Schekochihin, A. A., Cowley, S. C., Kulsrud, R. M., Hammett, G. W., & Sharma, P. 2005, ApJ, 629, 139
Schlickeiser, R. 2004, PhPl, 11, 5532
Schlickeiser, R. 2005, PPCF, 47, A205
Schlickeiser, R., Ganz, A., Kolberg, U., & Yoon, P. H. 2015, PhPl, 22, 102111
Stark, D. J., Bhattacharjee, C., Arefiev, A. V., et al. 2015, PhRvL, 115, 025002
Stenzel, R. L., Urrutia, J. M., & Strohmaier, K. D. 2007, PhRvL, 99, 265005
Summers, D., Thorne, R. M., & Xiao, F. 1998, JGR, 103, 20487
Tajima, T., & Taniuti, T. 1990, PhRvA, 42, 3587
Treumann, R. A., & Baumjohann, W. 2016, Ann. Geophys., 34, 737
Viñas, A. F., Moya, P. S., Navarro, R. E., et al. 2015, JGR, 120, 3307
Wardle, J. F. C., Homan, D. C., Ojha, R., & Roberts, D. H. 1998, Natur, 395, 457
Xiao, F., Thorne, R. M., & Summers, D. 1998, PhPl, 5, 2489
Yang, T. B., Gallant, Y., Arons, J., & Langdon, A. B. 1993, PhFlB, 5, 3369
Yoon, P. H. 1989, PhFlB, 1, 1336
Yoon, P. H. 1990, PhFlB, 2, 842
Yoon, P. H. 2007, PhPl, 14, 024504